Phosphorylation Alters the pH-Dependent Active State Equilibrium of Rhodopsin by Modulating the Membrane Surface Potential†

Scott K. Gibson, John H. Parkes, and Paul A. Liebman*

Department of Biochemistry and Biophysics, University of Pennsylvania Medical Center, Philadelphia, Pennsylvania 19104-6059

Received February 19, 1999; Revised Manuscript Received May 10, 1999

ABSTRACT: Phosphorylation reduces the lifetime and activity of activated G protein-coupled receptors, yet paradoxically shifts the metarhodopsin I−II (MI−MII) equilibrium (K_{eq}) of light-activated rhodopsin toward MII, the conformation that activates G protein. In this report, we show that phosphorylation increases the apparent p*K* for MII formation in proportion to phosphorylation stoichiometry. Decreasing ionic strength enhances this effect. Gouy−Chapman theory shows that the change in p*K* is quantitatively explained by the membrane surface potential, which becomes more negative with increasing phosphorylation stoichiometry and decreasing ionic strength. This lowers the membrane surface pH compared to the bulk pH, increasing K_{eq} and the rate of MII formation (k_1) while decreasing the back rate constant (k_{-1}) of the MI−MII relaxation. MII formation has been observed to depend on bulk pH with a fractional stoichiometry of 0.6−0.7 H^+/MII. We find that the apparent fractional H^+ dependence is an artifact of altering the membrane surface charge during a titration, resulting in a fractional change in membrane surface pH compared to bulk pH. Gouy−Chapman calculations of membrane pH at various phosphorylation levels and ionic strengths suggest MII formation behavior consistent with titration of a single H^+ binding site with 1:1 stoichiometry and an intrinsic p*K* of 6.3 at 0.5 °C. We show evidence that suggests this same site has an intrinsic p*K* of 5.0 prior to light activation and its protonation before activation greatly enhances the rate of MII formation.

Absorbed light can isomerize 11-*cis*-retinal, the resting state inverse agonist of rhodopsin, to the all-trans configuration, providing the agonist of visual transduction. The light-activated receptor quickly relaxes through several spectroscopically distinguishable intermediates, forming a quasi-equilibrium between two species, metarhodopsins I (MI,[1] λ_{max} 480 nm) and II (MII, λ_{max} 387 nm) (*1*). MII activates the retinal rod G protein, transducin (*2*−*4*).

The equilibrium between MI and MII is affected by several factors including pH. MII formation is known to be accompanied by proton uptake, but the stoichiometry of this uptake is puzzling in that it is apparently less than 1:1 (*1*, *5*, *6*). Thus, in Scheme 1, *n* has the value of 0.6−0.7.

Scheme 1

$$\mathrm{Rh} \xrightarrow{\text{light}} \mathrm{MI} + n\mathrm{H}^+ \underset{k_{-1}}{\overset{k'_1}{\rightleftharpoons}} \mathrm{MII}$$

Regulation of the lifetime and activity (quenching) of activated G protein coupled receptors (GPCR) by phosphorylation was first described for rhodopsin (*7*−*9*), which is multiply phosphorylated on C-terminal serine and threonine residues by rhodopsin kinase, GRK1 (*10*−*12*). Phosphorylation decreases the ability of rhodopsin to activate G protein (*13*) and facilitates the binding of arrestin (*14*), which enhances the inhibitory effect (*15*).

We have recently reported that the MI−MII equilibrium (K_{eq}) shifts toward MII in proportion to phosphorylation stoichiometry in native rod disk membranes (RDM) (*16*). A previous study reported K_{eq} to be unaffected by phosphorylation for rhodopsin reconstituted into POPC liposomes (*17*). This suggests that MII stabilization by phosphorylation is dependent on properties of RDM that are absent from POPC.

Rhodopsin inserts unidirectionally in RDM and bidirectionally in liposomes. Rhodopsin's dipolar charge distribution is such that its bidirectional insertion into PC liposomes yields a membrane net surface charge near zero (*18*). Inclusion of PS in liposomes augments negative membrane surface charge, which increases K_{eq} to more RDM-like values (*19*). A more negative surface produces a lower membrane surface pH, favoring MII formation. These and other effects imply that the increase in local negative charge density upon rhodopsin phosphorylation increases K_{eq} in RDM, while this effect is absent in PC vesicles because of lower membrane surface charge density.

Gouy−Chapman theory relates membrane surface charge density to membrane surface potential (*20*); this relationship successfully explains several biological membrane phenomena (*21*−*26*). The membrane surface potential of RDM and of rhodopsin liposomes has been measured with phospho-

† Supported by NIH Grants EY00012, EY01583, and EY07035.

* Address correspondence to this author: Telephone 215-898-6917; FAX 215-573-8093; Email liebmanp@mail.med.upenn.edu.

[1] Abbreviations: MI, metarhodopsin I; MII, metarhodopsin II; MIII, metarhodopsin III; RDM, rod disk membrane; K_{eq}, MII/MI equilibrium constant; λ_{max}, maximum absorbance wavelength; GPCR, G protein-coupled receptor; GRK, G protein receptor kinase; OD, optical density; EDTA, ethylenediaminetetraacetic acid; NADPH, β-nicotinimide adenine dinucleotide phosphate, reduced form; DTT, dithiothreitol; POPC, 1-palmitoyl-2-oleoyl-*sn*-glycero-3 phosphocholine; PC, phosphatidylcholine; PS, phosphatidylserine; pK_{app}, apparent p*K*; pK_i, intrinsic p*K*; pH_{memb}, membrane surface pH; k_{obs}, observed rate constant.

10.1021/bi990411w CCC: $18.00 © 1999 American Chemical Society
Published on Web 07/29/1999

nium spin labels (*18*). A Gouy−Chapman model was used to quantitatively describe the ionic strength and PS concentration dependence of the measured membrane surface potential, indicating that the charges on rhodopsin are located near the surface and can be described by the smeared charge surface required by the Gouy−Chapman theory.

In this report, we show that the apparent p*K* (pK_{app}) for MII formation increases directly with rhodopsin phosphorylation and inversely with ionic strength. The magnitude of these effects is well described by a Gouy−Chapman formulation that relates RDM surface pH to membrane surface potential. The apparent fractional H^+ stoichiometry previously observed for MII formation is explained as an effect of membrane surface potential. When corrected for this effect, our analysis shows MII formation to be accompanied by the uptake of a single proton (1:1 stoichiometry).

EXPERIMENTAL PROCEDURES

Preparation of Rod Disk Membranes. RDM were purified from bovine eyes obtained from a local slaughterhouse as previously described (*27*). The rhodopsin concentration was determined from its absorption spectrum by using the Dartnall correction for light scattering[2] (*28*).

Preparation of Phosphorylated Rhodopsin. Rhodopsin samples with increasing average phosphorylation stoichiometries were produced as previously described (*16*). The RDM were hypotonically stripped after phosphorylation to remove peripheral membrane proteins (*9*) and finally suspended in 10 mM $KHPO_4$, 25 mM KCl, 0.01 mM EDTA, and 1 mM DTT at a stock concentration of about 200 μM. These samples were purged with argon and stored in dark containers on ice. During the preparation procedure, samples were washed three times in 0.1 mM EDTA, once in 20 mM EDTA (overnight incubation), and three times in 1 mM EDTA. After this process, these samples were assumed to be free of divalent metals.

Measurement of MII Formation. Nineteen light flashes of equal intensity separated by 50 s intervals were used to bleach 3−4% of the remaining rhodopsin per flash (*29*). MII formation was continuously measured at 390 nm while the absorbance of the MI−MII isosbestic point (426 nm) was subtracted to correct for changes in light scattering (*30*). Data were taken every 4 ms and averaged and stored every 16 ms.

Spectral data were acquired with a SLM/Aminco DW2000 dual-wavelength spectrophotometer (Urbana, IL) equipped with a thermally jacketed cuvette holder connected to a constant-temperature water circulator. All measurements were made in quartz cuvettes with a 1 cm path length (measuring beam axis) and a width of 0.4 cm (bleaching axis). Bleaching flashes were produced by an EG&G Electro Optics (Salem, MA) xenon flash unit (FX-199 tube, PS-302 power supply set at 500 V, with a 7 μF external capacitor) outfitted with optical filters to limit the bleaching flash to wavelengths between 420 and 680 nm. The exact concentration of rhodopsin (around 10 μM) was measured for each experimental sample. Measurements were made at 0.5 ± 0.1 °C to minimize the gradual decay of MII into MIII (λ_{max} ∼ 460 nm) during the course of an experiment.

[2] $[Rh] = (1.10OD_{500} - 0.77OD_{600} - 0.33OD_{400})/40\,000\ cm^{-1}\ M^{-1}$.

Determination of MII Formation Parameters. The MI−MII equilibrium constant, K_{eq}, and the fraction of rhodopsin bleached per flash were determined from each 19-flash series as previously described (*16*, *29*). Briefly, this method assumes that light-activated rhodopsin consists only of MI and MII at equilibrium. According to Scheme 1, at constant pH

$$K_{eq} = \frac{[MII]}{[MI]} = \frac{k_1}{k_{-1}} \quad (1)$$

The pseudo-first-order rate constant, k_1, is related to the true second-order rate constant, k_1', by

$$k_1 = [H^+]^n k_1' \quad (2)$$

with *n* being the number of protons taken up in the reaction.

The changes in equilibrium ODs following each flash (ΔOD) were fit to the following equation by a nonlinear least-squares fitting algorithm:

$$\Delta OD = \Delta[MI]\Delta\epsilon_{Rh\rightarrow MI} + \Delta[MII]\Delta\epsilon_{Rh\rightarrow MII} \quad (3)$$

where Δ[MI] and Δ[MII] are the concentrations of MI and MII formed per flash, and $\Delta\epsilon_{Rh\rightarrow MI}$ (−7200 M^{-1} cm^{-1}) and $\Delta\epsilon_{Rh\rightarrow MII}$ (34 800 M^{-1} cm^{-1}) are the Rh → MI and Rh → MII differential extinction coefficients, respectively.

To improve the signal-to-noise ratio for kinetic resolution of MII formation, the last 17 responses in a 19-flash series were averaged into a single flash response.[3] The averaged response was well fitted by a single rising exponential of observed rate constant k_{obs}. Pseudo-first-order forward (k_1) and reverse (k_{-1}) rate constants contributing to k_{obs} were determined as previously described (*6*). Briefly, k_1 was determined from k_{obs} by

$$k_1 = \frac{k_{obs}\Delta OD}{\Delta\epsilon_{MI\rightarrow MII}[Rh^*]} \quad (4)$$

where Rh* is the concentration of activated rhodopsin, Δ*O*D is the change in optical density associated with the MI→MII transition, and $\Delta\epsilon_{MI\rightarrow MII}$ (42 000 M^{-1} cm^{-1}) is the MI → MII differential extinction coefficient. At low pH, where the increase in OD following a flash partitions into a fast and slow phase, k_{obs} was determined from the exponential fit of the slow phase. Equation 4 was used to determine k_1, using a value of ΔOD that is the increase from the calculated OD for complete MI conversion to the final OD of the flash response at equilibrium. This is equivalent to using the concentration of Rh* that progressed through the slow phase but is much easier to calculate.

Buffers and pH Determination. The pH of each RDM sample was set approximately by diluting 25 μL of RDM stock with 475 μL of solution buffered to a desired pH. The following buffers were used for the indicated pHs: potassium acetate (pH ∼ 5.0), 2-(*N*-morpholino)ethanesulfonic acid (MES; pH ∼ 5.5−6.5), 3-(*N*-morpholino)propanesulfonic acid (MOPS; pH ∼ 7.0−7.5), *N*-(2-hydroxyethyl)piperazine-*N*′-2-ethanesulfonic acid (HEPES; pH ∼ 8.0), and *N*-tris-(hydroxymethyl)methyl-3-aminopropanesulfonic acid (TAPS;

[3] The first two flashes were not fit because of distortion by residual G protein that stabilizes MII.

pH ~ 8.5−9.5). The exact pH of each sample was measured using an Orion 81−03 semimicro Ross electrode (Boston, MA) following each experiment. The pH measurements were made either on ice (~0 °C) or at room temperature with extrapolation to the experimental temperature (0.5 °C) by use of the thermal dependence of the p*K* for each buffer (*31*); results from these two methods were in good agreement.

Ionic Strength Assignments. Zwitterionic amines were assumed not to contribute to the overall ionic strength. In their unprotonated form, however, zwitterionic buffers are anions with potassium (K^+) as counterion. The amount of each buffer anion was therefore calculated from its p*K* and total concentration and used as its ionic strength contribution. Buffer concentration was 10 mM for solutions of 25 or 100 mM total ionic strength, and 5 mM for solutions of 10 mM total ionic strength. The 25 μL of RDM stock used for each experiment was calculated to contribute 2 mM K^+ to the 500 μL experimental sample. The remaining ionic strength contribution came from additions of KCl calculated to give a desired overall ionic strength.

pH Dependence of MII Formation. The 19-flash method was used to determine K_{eq} at each pH. The pH dependence of K_{eq} was plotted as the fractional amount of MII versus pH:

$$\text{fraction in MII} = \frac{\text{MII}}{\text{MI} + \text{MII}} = \frac{K_{eq}}{1 + K_{eq}} \quad (5)$$

Each resulting titration curve was fitted to the following Henderson−Hasselbalch equation, which allowed the proton stoichiometry, *n*, and titration end points, ep, to vary:

$$\frac{\text{MII}}{\text{MI} + \text{MII}} = \frac{\text{ep1} + (\text{ep2})10^{\text{p}K - n\text{pH}}}{1 + 10^{\text{p}K - n\text{pH}}} \quad (6)$$

where ep1 is the lower and ep2 is the higher end point.

Membrane Surface Potential and pH. Membrane surface potential was calculated from the Gouy−Chapman equation:

$$\sigma = (C^{1/2}/A) \sinh (ZF\Psi_0/2RT) \quad (7)$$

where σ is membrane surface charge density, Ψ_0 is membrane surface potential, *C* is salt concentration, *Z* is salt valence, and *A* is 134.8 $M^{1/2}$ Å^2 at 0.5 °C (*20*). Membrane surface pH is related to membrane surface potential and bulk pH by the Nernst equation:

$$\text{pH}_{\text{memb}} = \text{pH}_{\text{bulk}} + F\Psi_0/(2.303RT) \quad (8)$$

Membrane surface charge density (σ) depends on the number and p*K*s of ionizable groups at the cytoplasmic membrane surface and upon the membrane surface pH. The RDM surface area for a rhodopsin unit cell is approximately 4000 Å^2 (*32*). The numbers of ionizable amino acids and PSs previously employed to model the RDM surface potential (*18*) were used in our calculations (Table 1). Average amino acid p*K*s in proteins (*33*) were extrapolated to 0.5 °C by use of the thermal dependence of the p*K*s of the free amino acids (*34*). Glu-134 is thought to be the MII protonation site (*35*). The p*K* for Glu-134 is inferred to be approximately 6.2 on the basis of previous measurements of the p*K* for MII formation (*29*) corrected for the RDM surface potential. The p*K* of the PS carboxyl group is 3.6 (*36*). PS also binds K^+ with a dissociation constant (K_{salt}) of 6.7 M (*37*).

Table 1: Number of Charged Groups and Their Intrinsic pK on the Cytoplasmic Membrane Surface of a Rhodopsin Unit Cell

charged groups	number on surface[a]	pK^b (0.5 °C)	charged groups	number on surface[a]	pK^b (0.5 °C)
Arg	5	11.2	Glu (ERY)	1	6.2[c]
His	2	6.3	Tyr	2	9.4
Lys	9	9.3	α-COOH	1	3.1
Asp	2	4.4	PO_4 (pK_1)	0−9	3.0[c]
Cys	2	8.2	PO_4 (pK_2)	0−9	6.5[c]
Glu	7	4.4	PS	8	3.6[d]

[a] Ref 18. [b] From ref 33 and temperature corrected to 0.5 °C using the thermal dependence of the p*K*s (ref 34). [c] Estimated values. [d] Ref 36.

The contribution of each amino acid to the membrane surface charge density was determined from its p*K* and the membrane surface pH. The charge contribution of basic amino acids is

$$\sigma_{\text{basic}} = N/(1 + 10^{\text{pH}_{\text{memb}} - \text{p}K}) \quad (9)$$

and that of acidic amino acids is

$$\sigma_{\text{acidic}} = N[1 - 1/(1 + 10^{\text{pH}_{\text{memb}} - \text{p}K})] \quad (10)$$

The charge contribution from PS depends on the membrane surface concentration of both K^+ and H^+. The membrane surface charge density for PS was calculated from (*36*)

$$\sigma_{\text{PS}} = \frac{N}{1 + \left(\frac{[\text{H}^+]}{K_{\text{H}}} + \frac{[\text{K}^+]}{K_{\text{salt}}}\right) \exp\left(-\frac{F\Psi_0}{RT}\right)} \quad (11)$$

where *N* is the total surface density of each ionizable group per square angstrom, K_{salt} is the dissociation constant of K^+ for PS, K_H is the dissociation constant for H^+ ($10^{-\text{p}K}$), and $[H^+]$ and $[K^+]$ are bulk concentrations. The total charge density per rhodopsin unit cell is

$$\sigma = \Sigma\sigma_{\text{basic}} - \Sigma\sigma_{\text{acidic}} - \sigma_{\text{PS}} \quad (12)$$

Membrane surface concentration of both H^+ and K^+ depends on membrane surface potential. These surface concentrations in turn determine the membrane surface charge density. Thus, iterative computations were needed to solve these equations for the membrane surface pH. Initially pH_{memb} was assumed to be the same as bulk pH, and the surface charge density was calculated using from eqs 9−12. Equation 7 was then solved for Ψ_0, and eq 8 provided a new estimate for pH_{memb}. The process was repeated until self-consistency was obtained.

RESULTS

Effect of Phosphorylation and Ionic Strength on K_{eq}. We previously showed that rhodopsin phosphorylation increased K_{eq} in proportion to phosphorylation stoichiometry and did not change the fraction of rhodopsin bleached per flash (*16*). This effect is shown in Figure 1. Decreasing ionic strength increased the $OD_{390-426\ nm}$ per flash (Figure 1A) without altering the fraction of rhodopsin bleached per flash (Figure

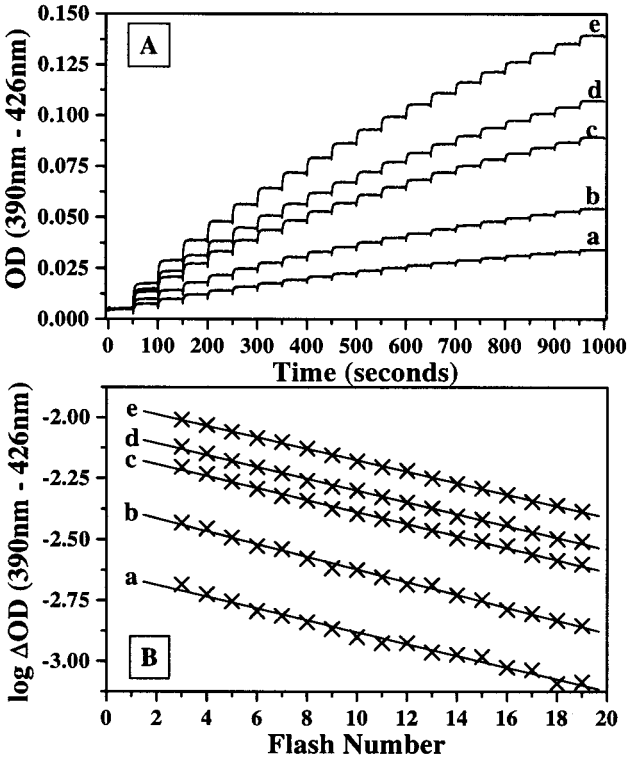

FIGURE 1: Response to 19 serial flashes of constant intensity for samples with (a) 0.0, (b) 2.4, and (c−e) 6.2 phosphates per rhodopsin. The monovalent ionic strength for each sample was (a−c) 100 mM, (d) 25 mM, and (e) 10 mM. (A) MII formation was monitored at 390−426 nm at 0.5 °C. All data have been normalized to 9 μM rhodopsin. (B) Change in optical density between flashes from panel A, corrected for MIII formation and plotted on a log scale. The first two points are not shown due to increased ΔOD due to MII enhancement by residual G protein. The linearity of the data shows that the fraction of rhodopsin bleached per flash is constant. The similar slope of all the data shows that the fraction bleached is not dependent on phosphorylation or ionic strength.

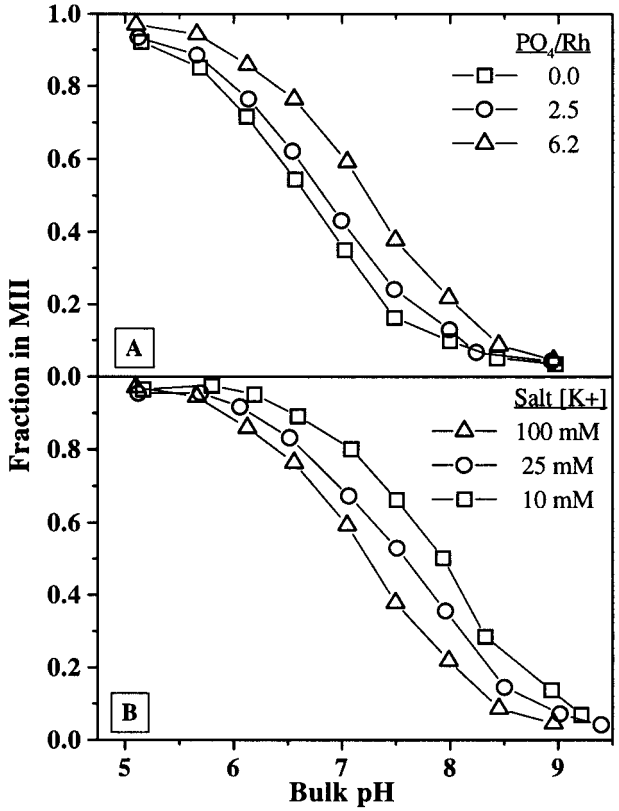

FIGURE 2: pH titration of MII formation. (A) Samples with increasing phosphorylation stoichiometry in 100 mM ionic strength medium. The apparent p*K* for MII formation increases with phosphorylation. (B) Ionic strength dependence of MII formation for rhodopsin with 6.2 phosphates. Decreasing ionic strength increases the apparent p*K*.

1B). This shows that both increasing phosphorylation and decreasing ionic strength increase K_{eq}.

Rhodopsin phosphorylation caused the apparent p*K* (pK_{app}) for MII formation to shift to more alkaline pH, the magnitude of the shift increasing with increasing phosphorylation stoichiometry (Figure 2A). In 100 mM ionic strength medium, pK_{app} shifted from 6.7 for unphosphorylated rhodopsin to 7.3 for samples with 6.2 phosphates/rhodopsin. At lower ionic strength, the pK_{app} shift was enhanced (Figure 2B). pK_{app} for samples with 6.2 phosphates/rhodopsin shifted from 7.3 to 7.9 when ionic strength was reduced from 100 to 10 mM.

The effect of increasing phosphorylation on K_{eq} and its enhancement at reduced ionic strength suggests that phosphorylation alters K_{eq} by increasing the negative membrane surface potential of the cytoplasmic (extradiskal) surface. The negatively charged surface attracts H^+ ions, lowering the membrane surface pH (pH_{memb}; eq 8). Gouy−Chapman calculations were used to determine whether alterations in phosphorylation stoichiometry and/or ionic strength could produce changes of pH_{memb} that account for the shift in the apparent p*K* of MII formation.

MII titration curves for three different phosphorylation stoichiometries and three different ionic strengths are shown in Figure 3A. Each of the nine curves has a different pK_{app}. These nine curves were brought into congruence by application of the iterative Gouy−Chapman calculation (see Experimental Procedures), thus showing that their salt and phosphorylation dependence is quantitatively explained by changes in pH_{memb} at the cytoplasmic surface (Figure 3B). All consequent plots with pH_{memb} as titration variable overlay each other with an intrinsic p*K* (pK_i) of 6.3 for MII formation.

Fractional Proton Stoichiometry. Henderson−Hasselbalch fits (eq 6) to the bulk pH MII titration curves (Figure 3A) gave *n* values around 0.7 (Table 2) in agreement with previous reports (*1*, *5*, *6*). Fits to pH_{memb} titration plots (Figure 3B), however, gave *n* values approaching 1 (Table 2). This is consistent with the reaction model shown in Scheme 1 with a single proton accompanying MII formation.

Kinetic Analysis. The pH dependence of the kinetics of MII formation has been studied with unphosphorylated rhodopsin (*6*, *38*). An ionic strength dependence of MII formation has also been reported (*39*). However, there has been no previous investigation of the effect of phosphorylation on these parameters.

The effect of pH on the observed rate constant for MII formation (k_{obs}) at various phosphorylation levels and ionic strengths is shown in Figure 4A. Both ionic strength and phosphorylation affect k_{obs}. The previously reported U-shaped pH dependence of k_{obs} (*6*) was maintained for all conditions with a minimum around pH 7 for unphosphorylated rhodopsin. Increasing phosphorylation and decreasing ionic strength shift the entire k_{obs} curve to higher pH. In 10 mM ionic strength buffer, the pH minimum of k_{obs} for samples with 6.2 phosphates/rhodopsin was shifted almost 1 pH unit to

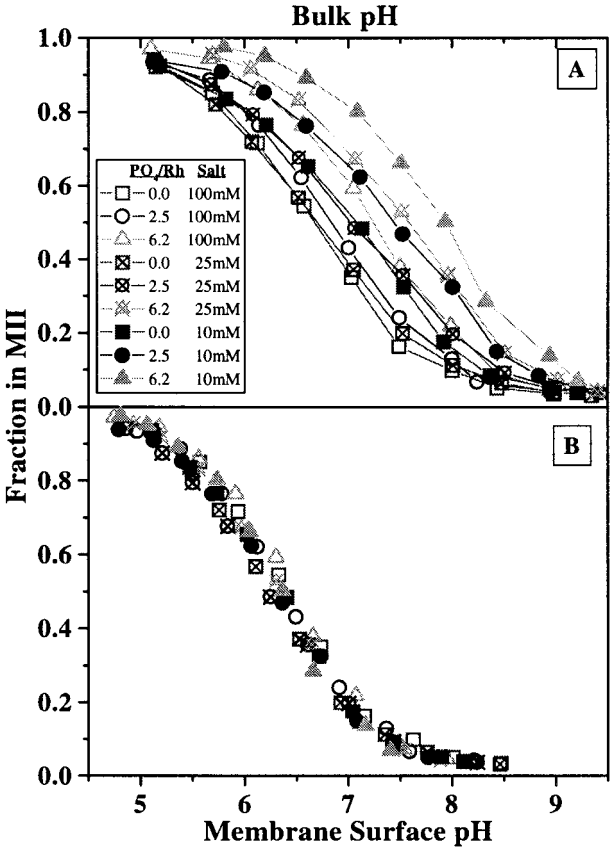

FIGURE 3: pH dependence of MII formation at 0.0, 2.5, and 6.2 phosphates/rhodopsin in media of 100, 25, and 10 mM ionic strength. (A) Bulk pH titration of MII formation. Curves are shifted by phosphorylation stoichiometry and ionic strength. (B) Titration data as a function of calculated membrane surface pH. The curves overlay each other and appear to be independent of phosphorylation stoichiometry and ionic strength.

Table 2: Best *n* Values of Henderson−Hasselbalch (eq 6) Fits for MII Formation as Function of Bulk or Membrane pH

PO_4/Rho	salt (mM)	best *n* from bulk pH	best *n* from membrane pH
0.0	100	0.85 ± 0.09	0.95 ± 0.11
2.5	100	0.80 ± 0.07	0.95 ± 0.09
6.2	100	0.76 ± 0.07	0.95 ± 0.10
0.0	25	0.69 ± 0.04	0.88 ± 0.07
2.5	25	0.61 ± 0.05	0.80 ± 0.07
6.2	25	0.72 ± 0.09	0.90 ± 0.13
0.0	10	0.73 ± 0.10	0.93 ± 0.14
2.5	10	0.65 ± 0.08	0.87 ± 0.12
6.2	10	0.80 ± 0.13	1.02 ± 0.24

7.9 compared to unphosphorylated rhodopsin at 100 mM ionic strength. At high pH (pH > 8.5), k_{obs} was unreliable because too little MII was formed.

Previous work has demonstrated that reduced pH increases the rate of MII formation (k_1) while decreasing its back rate to MI (k_{-1}) (*6*). Phosphorylation has the same effect as lower pH, increasing k_1 and decreasing k_{-1} (*16*). Figures 5A and 6A show that increasing phosphorylation and decreasing ionic strength augment the effect of bulk pH on k_1 and k_{-1}.

Shifts in MI−MII equilibrium caused by changes in phosphorylation or ionic strength are adequately explained by changes in membrane surface potential (Figure 3). The same explanation should account for the effect of phosphorylation and ionic strength on the kinetic parameters k_{obs}, k_1, and k_{-1}. Previous studies of the pH dependence of MII kinetics refer only to bulk pH values (*6*, *38*). Since membrane surface pH can be much lower than bulk pH, earlier conclusions need to be refined.

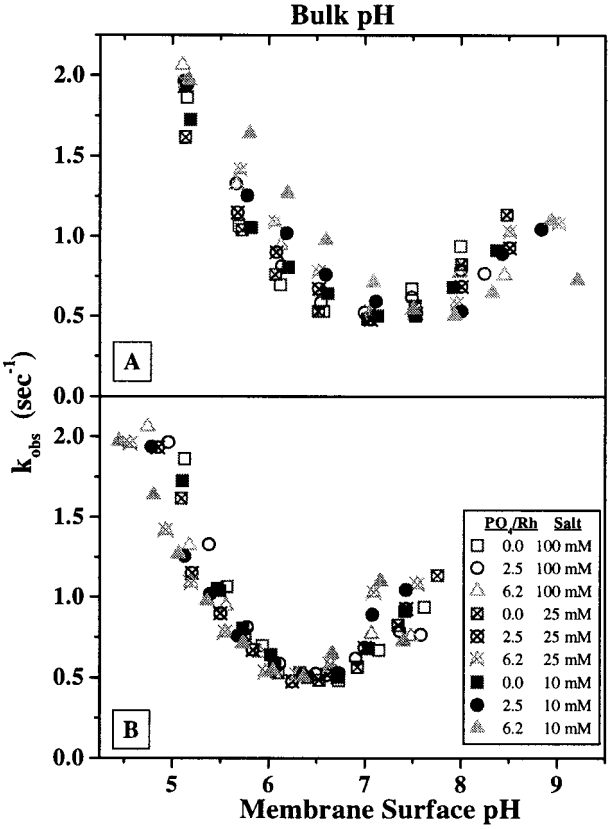

FIGURE 4: Dependence of the observed rate constant of MII formation (k_{obs}) on pH, ionic strength, and phosphorylation stoichiometry. (A) Bulk pH dependence of k_{obs} is U-shaped with a minimum that shifts with ionic strength and phosphorylation level. (B) Calculated membrane surface pH dependence of k_{obs}. Plots converge with a common minimum k_{obs} at membrane surface pH 6.4.

Membrane surface potential effects account for the phosphorylation and ionic strength dependence of k_{obs} (Figure 4B). The curves for all ionic strengths and phosphorylation levels overlay each other when plotted as a function of pH_{memb}. The shape of the pH dependence of k_{obs} remains U-shaped with a minimum at pH_{memb} 6.4. Membrane surface potential effects also explain the phosphorylation and ionic strength dependence of k_1 (Figure 5B) and k_{-1} (Figure 6B).

Values for K_{eq}, calculated as the ratio of kinetic constants k_1 and k_{-1}, are in excellent agreement with values determined from equilibrium analysis (Figure 7). Such agreement provides additional confidence that the measured values of k_{obs}, k_1, k_{-1}, and K_{eq} are correct.

The values of *n* taking pH_{memb} into account (Table 2) suggest that a 1:1 proton stoichiometry is required for MII formation. The true second-order forward rate constant, k_1', can thus be calculated by dividing the pseudo-first-order rate constant (k_1) by the membrane proton concentration (eq 2; $n = 1$). k_1' corrected for pH_{memb} (Figure 8) shows base catalysis, as was inferred from earlier bulk pH studies (*6*).

Fast-Forming Intermediate. At pH 6.5 and higher, a single rising exponential fits the kinetics of MII formation. At lower pH, this phase is progressively replaced by a much faster component (Figure 9). Formation of this fast phase must be

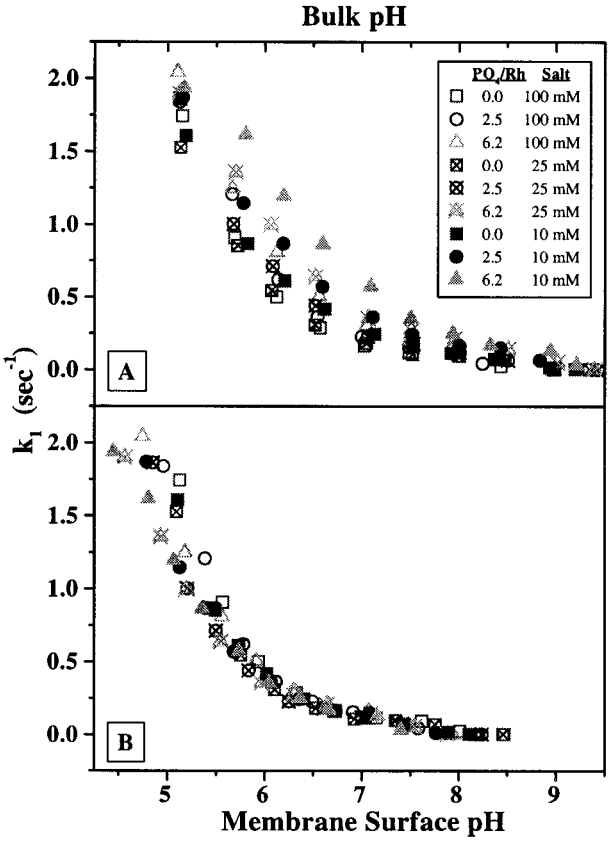

FIGURE 5: Dependence of the pseudo-first-order rate constant for MII formation (k_1) on pH, ionic strength, and phosphorylation stoichiometry. (A) Bulk pH dependence of k_1. k_1 increases with decreasing bulk pH and ionic strength and increasing phosphorylation. (B) Membrane surface pH calculations account for the phosphorylation and ionic strength dependence of k_1.

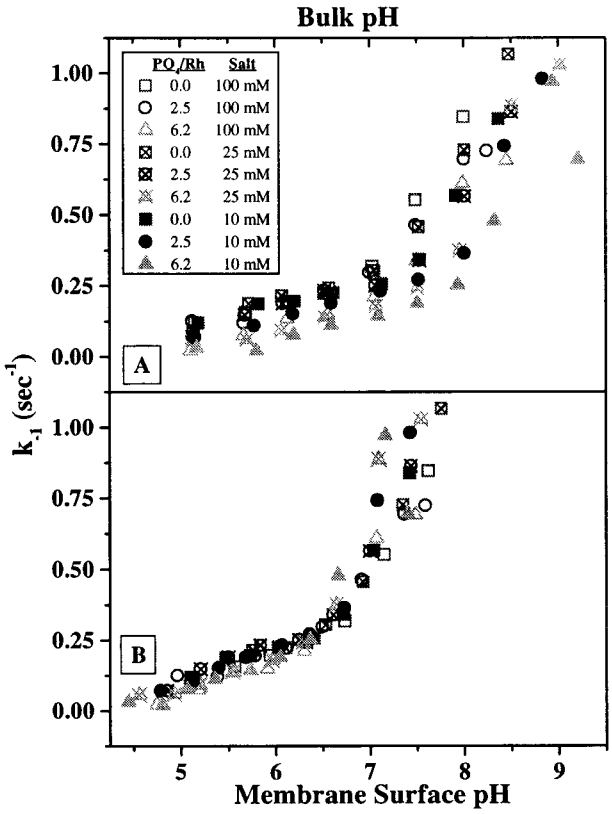

FIGURE 6: Dependence of the rate of MI formation from MII (k_{-1}) on pH, ionic strength, and phosphorylation stoichiometry. (A) Bulk pH dependence of k_{-1}. The reaction appears to be base-catalyzed and is decreased by increasing phosphorylation levels and decreasing ionic strengths. (B) Membrane surface pH calculations account for the phosphorylation and ionic strength dependence of k_{-1}.

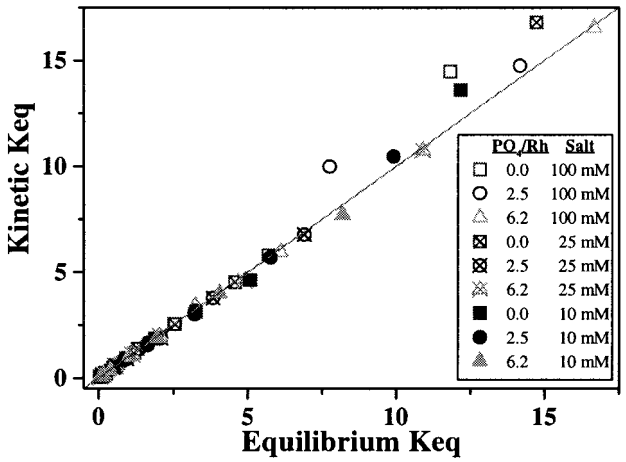

FIGURE 7: Agreement between K_{eq} values determined by equilibrium analysis and those calculated as the ratio of forward to reverse rate constants under various salt and phosphorylation conditions. The line has a slope of 1.

complete before our first postbleach measurement (4 ms),[4] given that a single rising exponential adequately fit the remainder of the flash response.

In determining the rate constants, k_1 and k_{-1}, from k_{obs}, we assumed that the final amplitude of the flash response was due only to MI and MII. This implies that the fast component relaxes into the classical MI−MII equilibrium with a time constant equal to k_{obs} at all pHs, preserving the single-exponential character of the slow phase. K_{eq} determined from the final amplitude of each flash response (equilibrium method) is in good agreement with kinetically determined values of K_{eq} (ratio of rate constants) (Figure 7). This agreement suggests that the kinetic assumptions are appropriate.

The fast-forming component increased with decreasing bulk pH and ionic strength and with increasing phosphorylation (Figure 10A). Its ionic strength and phosphorylation dependence is accounted for by changes of pH_{memb} (Figure 10B). A Henderson−Hasselbalch fit well described the pH_{memb} dependence of the fast-phase amplitude. The results are consistent with protonation of a single site with a pK_i of 5.0. The end point of the fit (ep2 in eq 6) is equal to the optical density calculated for complete MII formation (0.017 OD).

[4] The absorbance was sampled over 4 ms, averaged, and stored every 16 ms. Since the fast component appears to be complete by our first recorded point (16 ms), we can conclude that the four measurements that make up this point do not contain any of the fast component.

DISCUSSION

Despite the great diversity of agonists for G protein-coupled receptors, this family of receptors has many features in common. Much of the paradigm for GPCR signaling was first described in the rhodopsin system. The abundance of this receptor and its unique spectroscopic properties provides information about GPCR signaling that is either difficult or impossible to obtain for other members of the GPCR family.

The regulation of GPCR signaling by phosphorylation of the C-terminal tail of the receptor by a G protein receptor

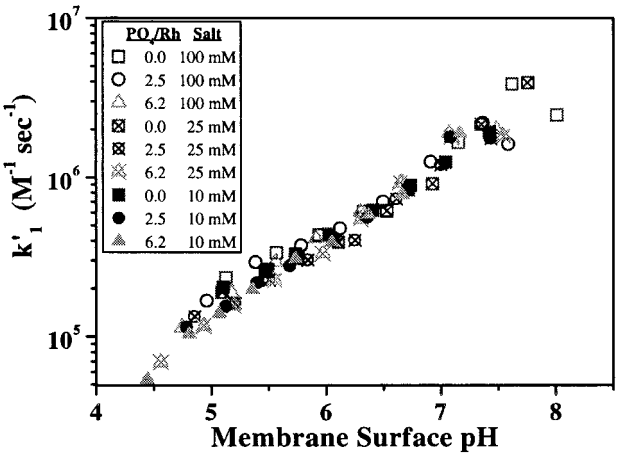

FIGURE 8: Dependence of the true forward rate constant, k_1', for MII formation on membrane surface pH. The calculation assumes that one proton is necessary for MII formation. The values for k_1' increase with membrane surface pH; therefore, k_1' is base-catalyzed.

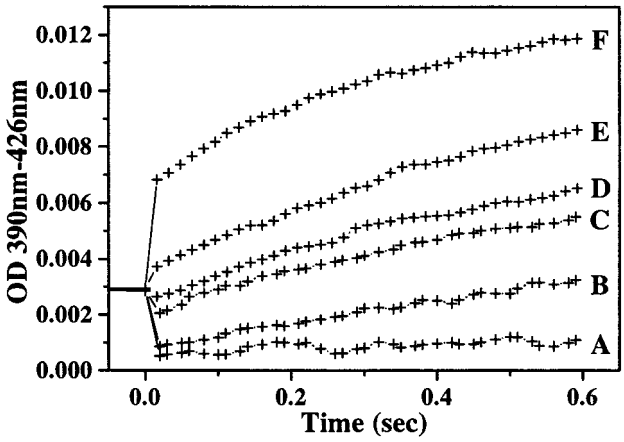

FIGURE 9: First 600 ms of the averaged flash response for the following samples: (A) 0.0 PO_4/Rh, pH 7.5; (B) 0.0 PO_4/Rh, pH 6.5; (C) 0.0 PO_4/Rh, pH 6.0; (D) 2.5 PO_4/Rh, pH 6.0; (E) 6.2 PO_4/Rh, pH 6.0; (F) 6.2 PO_4/Rh, pH 6.0. Data A−E were obtained in 100 mM ionic strength buffer, and data set F was measured in 10 mM ionic strength buffer. All data were normalized to a 10 μM rhodopsin concentration with a 4% bleaching flash. The flash occurred at time zero. The initial drop in OD for samples A−D was due to MI formation ($\Delta\epsilon_{Rh\rightarrow MI}$ −7200 M^{-1} cm^{-1}). Spectra C−F have a fast phase followed by a slower phase due to MII formation. The fast phase appeared complete by the our first measurement (4 ms) since the first averaged and stored data point of each set (16 ms) was not perturbed.

kinase (GRK) was first discovered in the rhodopsin system (*7*−*9*). Phosphorylation of rhodopsin reduces G protein activation (*13*), facilitates the binding of arrestin (*14*, *40*), and stabilizes the active conformation of rhodopsin, MII (*16*).

In this report, we show that rhodopsin phosphorylation stabilizes MII by shifting the apparent p*K* of MII formation to higher pH. The shift increases with increasing phosphorylation and decreasing ionic strength. Moreover, the rate of MII formation, k_1, increases with phosphorylation stoichiometry and decreasing ionic strength while the reverse rate, k_{-1}, has the opposite dependence, both defining the phosphorylation and ionic strength dependence of k_{obs} and K_{eq}.

Increasing phosphorylation and decreasing ionic strength shift the apparent p*K* for MII formation by increasing the negative membrane surface potential which, in turn, results

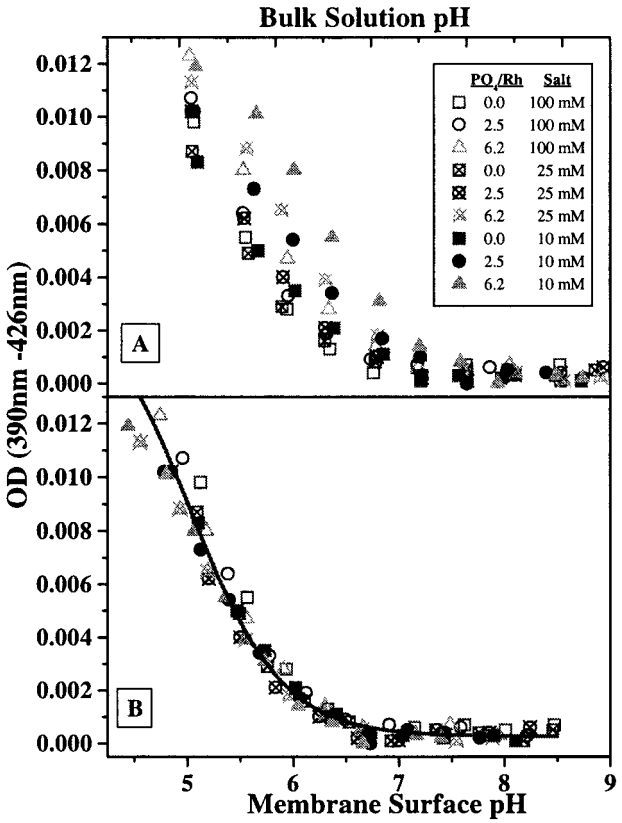

FIGURE 10: Effect of pH, ionic strength, and phosphorylation stoichiometry on the amplitude of the fast component. Zero amplitude was taken as the OD for 100% MI formation immediately following the flash (e.g., Figure 9, curve A). Fast-phase amplitude is the increase from this level to the value of the exponential fit to the slow phase, extrapolated back to the time of the flash. (A) Fast-phase amplitude increased with decreasing pH and ionic strength, and increasing phosphorylation. (B) Membrane surface pH calculations quantitatively account for the phosphorylation and ionic strength dependence of the fast-phase amplitude. A Henderson−Hasselbalch fit with $n = 1$ (solid line) to the pH_{memb} curve suggests that the fast phase depends on the protonation of a single site with an intrinsic p*K* of 5.0. At low pH, the fit saturates near the OD for complete conversion to MII.

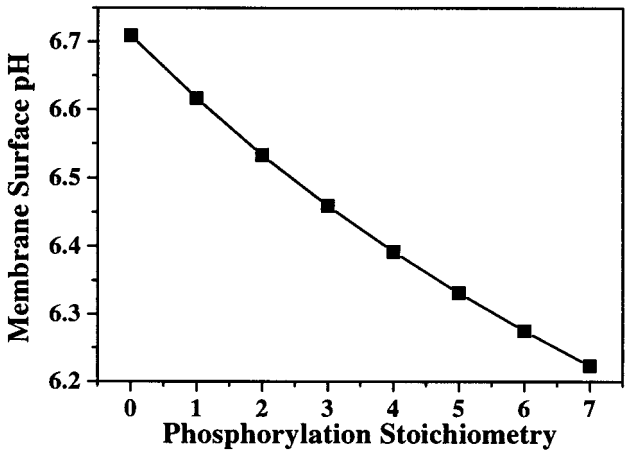

FIGURE 11: Calculated change in membrane surface pH with increasing phosphorylation at bulk pH 7.0 and 100 mM ionic strength at 0.5 °C. Lowering the ionic strength increases the slope of this relationship.

in a lower pH_{memb} (Figure 11). Our Gouy−Chapman calculations show that increasing phosphorylation augments the negative membrane surface charge density while decreasing

salt concentration reduces the electrostatic shielding of the surface charge; both conditions increase the negative surface potential magnitude. This model of the RDM surface quantitatively predicts phosphorylation and ionic strength dependence of K_{eq}, k_{obs}, k_1, and k_{-1}.

Previous investigations of the pH dependence of MII formation did not discriminate between pH_{memb} and bulk pH. It is clearly the local surface pH that is of consequence to a membrane-localized protein like rhodopsin. The difference between bulk pH and membrane surface pH can be substantial: up to 1.8 pH units at our most extreme condition (10 mM ionic strength and 6.2 phosphates/rhodopsin). Using Gouy−Chapman theory, we calculated pH_{memb} values corresponding to our bulk pH measurements. Henderson−Hasselbalch analysis of the pH_{memb} data shows that MII formation at 0.5 °C has an intrinsic p*K* of 6.3. This value is around 0.3 pH unit lower than previously reported bulk pH titration midpoints (*6*, *29*, *38*, *39*) extrapolated to 0.5 °C by use of the thermal dependence of MII formation (*6*).

The effect of cytoplasmic rhodopsin phosphorylation on K_{eq} demonstrates that MII formation is associated with cytoplasmic proton uptake in agreement with conclusions drawn from other studies (*35*, *41*, *42*). In addition, Gouy−Chapman calculations assuming intradiskal protonation failed to describe the ionic strength or phosphorylation dependence of MII titration curves (data not shown).

Physiological Relevance. We used rhodopsin that had been exhaustively bleached, phosphorylated to an average phosphorylation stoichiometry, and regenerated prior to our measurements. These steps produced a global change in the membrane charge density that could be modeled by the infinite plane of smeared charge required by the Gouy−Chapman equation.

Only a small fraction (<1%) of molecules are bleached in vivo, yielding a much lower density of phosphorylated rhodopsin compared to our in vitro system. The results from our Gouy−Chapman study, however, should still qualitatively hold true for in vivo physiology. Although phosphorylation of a single molecule will result in an imperceptible change in net membrane surface charge density, phosphorylation will increase the local negative potential around the molecule according to the Poisson−Boltzmann equation. This will cause a local redistribution of all mobile ions, including H^+, near the phosphorylated receptor, shifting its MI−MII equilibrium toward MII. In comparison, several studies of ion channels have demonstrated the importance of local electrostatics on ion concentration (*25*, *43*, *44*).

The stoichiometry of rhodopsin phosphorylation obtained in vivo is a highly debated subject. One report found only two phosphorylation sites in vivo (*45*). A more recent study, however, found three phosphates per rhodopsin in vivo (*46*). In addition, data from studies that mutated several combinations of rhodopsin phosphorylation sites suggest that multiple phosphorylation plays a role in arrestin binding (*47*, *48*). The question of physiological phosphorylation sites and stoichiometry is still unresolved. Even so, phosphorylation stoichiometries as low as one phosphate per rhodopsin will change the local electrostatic environment enough to alter MI−MII equilibrium.

Ionic Strength Effect. A previous study by Delange et al. (*39*) reported that increasing the ionic strength from ∼15 mM to 4 M raised the apparent p*K* of MII formation by about 3 pH units through a surface potential effect. Using a smaller range of ionic strengths (10−100 mM), our measurements demonstrate an opposite and weaker ionic strength dependence.

Increasing salt concentration can increase pK_{app} of MII formation through a surface potential effect only if the membrane surface has a net positive charge. Both intradiskal and extradiskal surfaces of RDM are negatively charged (*18*). Shielding of the membrane surface charge, regardless of its sign, should saturate as ionic strength is increased, resulting in pH_{memb} titration curves of MII formation that converge with increasing ionic strength. Indeed this is the case in our Figures 2B and 3A. Conversely, the titration curves of Delange et al. (*39*) diverge with increasing ionic strength. This suggests that their increase in K_{eq} with large changes in ionic strength is not due primarily to an effect on surface potential.

Increasing osmolality has previously been reported to increase K_{eq} (*49*). The increased osmolality was argued to favor MII formation by dehydrating the RDM. This effect would increase with salt concentration and would not saturate like a surface potential effect. Increased osmolality rather than a change in surface potential might be the source of the ionic strength effect observed by Delange et al.

Explanation of Apparent Fractional Proton Stoichiometry. Formation of MII is accompanied by deprotonation of the Schiff base of *all-trans*-retinal (*1*) and the uptake of a proton from solution (*50*) on the cytoplasmic side of the RDM. There is growing evidence that Glu-134 is the cytoplasmic protonation site (*35*, *51*−*54*); however, Fourier transform infrared spectroscopy (FTIR) studies have not detected protonation of this residue. In this paper, we refer to Glu-134 as the cytoplasmic protonation site since it is the leading candidate.

Previous observations suggest that only fractional proton stoichiometry is required for MII formation (*1*, *5*, *6*). The Schiff base proton is transferred internally to its counterion, Glu-113 (*55*−*57*), and is not thought to contribute to the pH dependence of MII formation. Therefore, MII's pH dependence must be attributed to the protonation of Glu-134.

Several explanations have been offered to account for the fractional value of *n*. It has been suggested that protonation of His-211 stabilizes MII while protonation of His-65 and His-152 destabilizes MII, creating an apparent fractional proton stoichiometry (*58*). Other studies propose that MII is in equilibrium with an additional 380 nm-absorbing intermediate that is pH-independent (*38*, *59*, *60*), thus giving an *n* value that equals the fraction of protonated MII.

Our work suggests a simpler explanation for a fractional *n*. As bulk pH is lowered in a titration, membrane charge density is reduced through protonation of titratable groups on the RDM surface (Figure 12A). The decrease in surface charge density lowers the membrane surface potential, thereby reducing the difference between the bulk and membrane surface pH (Figure 12B). This acts to extend the bulk pH range required to protonate Glu-134 beyond that which would have been required were the surface charge to remain fixed; thus creating the illusion that fractional proton stoichiometry is necessary for MII formation.

Table 2 supports this hypothesis. Henderson−Hasselbalch fits (eq 6) to the data of Figure 3A yield an average *n* of 0.73 as previously reported (*6*). We used our Gouy−

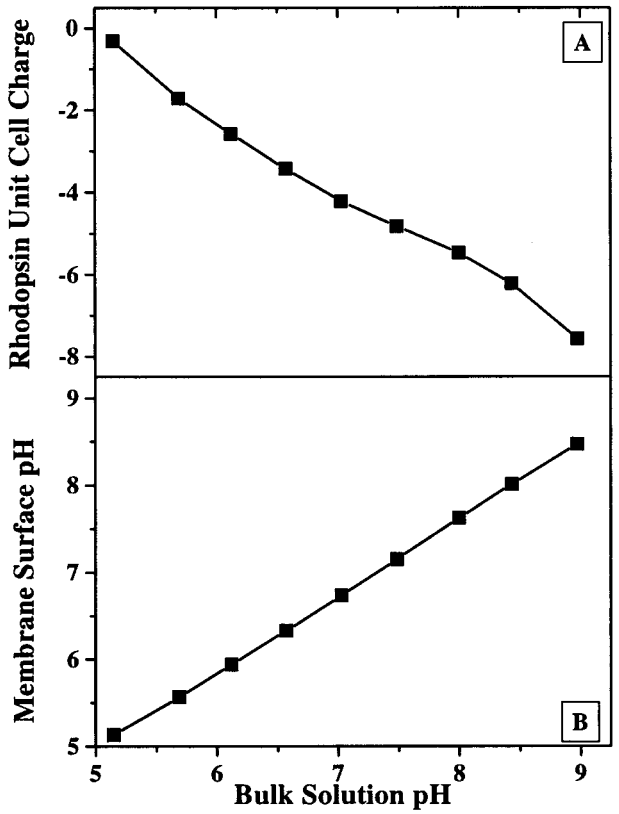

FIGURE 12: Effect of bulk pH on the membrane surface charge density and membrane surface pH with 100 mM monovalent salt at 0.5 °C. (A) Calculated change in rhodopsin unit cell charge with bulk pH. (B) Since the membrane surface charge density changes with pH, changing the bulk pH results in fractional changes in the membrane surface pH.

Chapman model together with the distribution of the charged residues and their p*K*s shown in Table 1 to compute the membrane surface pH corresponding to each value of bulk pH (Figure 3). Henderson−Hasselbalch fits to the pH_{memb} plots give an average *n* of 0.92. Though this model has potential sources of error (p*K*s may vary with local rhodopsin environment), the universal trend of the value of *n* toward 1 upon correction for local electrostatics strongly suggests that a single proton is associated with MII formation.

Other Roles for Surface Potential. Modifications of membrane surface potential will cause changes in the local membrane concentrations of all mobile ions. Local divalent cation concentrations have a much stronger dependence on membrane surface potential than monovalent ions (*20*, *21*); therefore, phosphorylation will strongly affect the membrane concentrations of metals such as Ca^{2+}, Mg^{2+}, Mn^{2+}, etc.

Divalent metals play several roles important to transduction mechanisms that may be influenced by phosphorylation effects on membrane surface potential. For example, Ca^{2+} is known to regulate rhodopsin kinase (*61*−*63*), guanylate cyclase (*64*), and Ca^{2+}-activated opsin phosphatase (*65*) activity. Due to the negative membrane surface potential of RDM, the Ca^{2+} concentration at the membrane surface will be higher than bulk concentration under all phosphorylation stoichiometries (0−9 phosphates/rhodopsin) and should be taken into account when Ca^{2+} binding constants of membrane proteins are determined and Ca^{2+}-specific effects are modeled.

PS Tunes the Membrane Surface Potential. The cytoplasmic surface of rhodopsin is positively charged in the absence of PS (Table 1). A positive membrane surface potential would cause the membrane surface pH to be higher than bulk pH, disfavoring MII formation. The concentration of PS is high enough on the cytoplasmic side of RDM to both counteract the positive charge of rhodopsin and to produce a net negative membrane surface charge (*18*). The resulting potential lowers pH_{memb}, favoring MII formation (increasing K_{eq}). Our calculations show that the PS in RDM lowers pH_{memb} by about 0.5 pH unit at 100 mM ionic strength and 0.5 °C.

pH-Dependent Pre-MII Intermediate. Below pH_{memb} 6.5, we detected a 390 nm-absorbing intermediate that formed with kinetics much faster than those of MII (Figures 9 and 10). Its rate of formation was too fast to be kinetically resolved by our apparatus. However, comparison of the equilibrium and kinetics of subsequent MII formation (slow phase) suggests that this fast-forming intermediate relaxes into the classical MI−MII equilibrium (Scheme 1). Given that (1) the slower phase was well fit by a single rising exponential at all pHs, (2) the total postflash absorbance plotted against pH_{memb} was well fit by a Henderson−Hasselbalch curve with an *n* of 1, and (3) there was excellent agreement between the values for K_{eq} obtained from kinetic and equilibrium measurements, it appears that the fast phase is due to accelerated formation of MII from a portion of the bleached rhodopsin.

Several groups have recently postulated the existence of 380 nm-absorbing species that appear before classical MII: MII_{fast} (*66*), MII_a (*59*, *67*, *68*) and MI_{380} (*38*, *60*). Formation of MI_{380} is thought to be pH-independent, while formation of MII_a appears to be pH-dependent in RDM (*68*) but not in detergent (*59*). The rate of formation of MII_{fast} was approximately the same as MII at temperatures below 20 °C. Similarly, the temperature dependence of MI_{380} suggests that it does not exist at the low temperatures (0.5 °C) of our study (*60*).

At pH ≤ 4 and pH ≥ 7.5, Dickopf et al. (*68*) reported that a single exponential adequately fit the kinetics of MII formation. At pHs between these extremes, two exponentials were required to fit the kinetic data. They assumed the two exponentials resulted from sequential formation of two isochromic species of MII, MII_a (fast component) and MII_b (slow component); this model is similar to the one proposed by Arnis and Hofmann (*59*).

The microscopic rate constants were determined by Dickopf et al. using this model, with the constraint that only one rate constant is pH-dependent, even though they found both the rates of MII_a and MII_b formation increased with decreasing pH. The model describing the rate of MII_b formation as pH-dependent failed to describe the data; this conclusion appears to disagree with all other kinetic studies, which show that a component analogous to the slow phase is dependent on pH (*6*, *38*, *39*, *69*, *70*). The alternative model describing the rate of MII_a formation as the pH-dependent component was able to fit the data at pHs below 7.5; at higher pHs the model failed. A model describing both MII_a and MII_b formation as pH-dependent and other possible kinetic schemes were not tested by these authors.

Although complete kinetic and thermodynamic characterization of the fast component in our low-pH measurements was beyond the scope of the present study, the pH dependence of the amplitude of our fast phase (Figure 10) is similar

Scheme 2

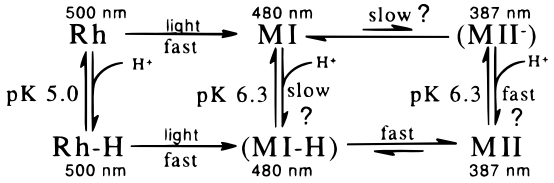

to the pH-dependent amplitudes of MII_a described by Dickopf et al. In addition, the measured rate of formation of this intermediate ($\sim$100−400 s^{-1} at 0.5 °C depending on pH) is fast enough to explain our results (>250 s^{-1}). In contrast to the model proposed by Dickopf et al., the kinetics of our slow phase (k_1) is also pH-dependent.

We propose that our fast phase might be due to protonation of Glu-134 prior to activation, allowing light-activated rhodopsin to proceed more rapidly to MII through the lower path in Scheme 2. In this model, the pK_i for Glu-134 would shift from 5.0 (Figure 10) in the dark-inactive state to 6.3 (Figure 3) in the light-activated state, accounting for the pH dependence of the fast and slow phases of MII formation. It is probable that the "fast" MII is identical to "classical" MII and that it does not have access to a fast path back to MI. It will relax back to the MI−MII equilibrium with the same k_{obs} seen in the normal (slow phase) production of MII. This is entirely consistent with our data and the results reported by Dickopf et al. (*68*).

In our fast phase, protonation of Glu-134 would appear to precede Schiff base deprotonation. If this order of protonation were to be preserved for the slow phase, MII would be formed through a slowly protonated 480 nm intermediate (MI-H in Scheme 2). This implies that events associated with the 11-cis to all-trans isomerization of the chromophore may quickly raise the p*K* of Glu-134. The shift in p*K* would favor protonation of Glu-134, which, according to this reaction path, is required for the deprotonation of the *all-trans*-retinal Schiff base linkage.

If the protonation order observed for the fast phase were not maintained for the slow phase, MII might be produced through a slowly forming unprotonated 387 nm intermediate (MII^- in Scheme 2), corresponding to the MII_a proposed by Arnis and Hofmann (*59*). MII would then form by fast protonation of MII^-. This reaction path suggests that deprotonation of the *all-trans*-retinal Schiff base linkage is required to raise the p*K* of Glu-134, favoring its protonation and thus stabilizing the unprotonated Schiff base.

Our results do not rule out either potential pathway (marked with question marks in Scheme 2) or specifically support the existence of MI-H or MII^-. However, our present work is consistent with protonation of Glu-134 before Schiff base deprotonation (fast phase). In addition, our finding of an *n* near 1 (Table 2) suggests that neither MI-H nor MII^- can be significantly populated nor can they be equally populated at equilibrium, since this is unlikely to be possible at all pHs.

If Glu-134 is protonated in its ground state with a p*K* of 5, there should be less proton uptake per MII formed at sufficiently low pH. Only a few studies have measured direct protonation at low enough pHs to see this effect. The results from these studies seem somewhat ambiguous.

Using an electrode to measure proton uptake, Bennett found decreased proton uptake per MII formed at pHs below 6 (*71*); the author noted that this may be due to "partial protonation of rhodopsin before bleaching". McConnell et al. (*72*) found a similar effect; however, Bennett found uptake of 2 H^+/MII, while McConnell et al. found uptake of 1 H^+/MII. On the other hand, a subsequent study by Bennett used the pH indicator dye bromocresol purple (p*K* 6.2), which showed the uptake of 2 H^+/MII formed at pHs 5−8 (*42*). At pH 4.5, however, the uptake of only 1 H^+/MII was found with digitonin-extracted rhodopsin and the pH indicator dye bromocresol green (p*K* 4.7) (*73*).

Cooper and Converse (*74*) measured the net proton uptake at pH 5.4 by comparing the enthalpy of MII formation in acetate (ΔH = 10.6 kcal/mol) with that in piperazine (ΔH = 17.2 kcal/mol). The ΔH variation of 6.6 kcal/mol is due to the difference between the heat of protonation of acetate (ΔH = 0 kcal/mol) and piperazine. The authors used a ΔH of −7.1 kcal/mol for piperazine and concluded that the protonation stoichiometry is near 1. A more recent value for ΔH of piperazine is −10.2 kcal/mol (*75*). Our recalculation of the protonation stoichiometry with this newer ΔH yields an uptake of 0.65 H^+/MII. According to our model and the data in Figure 10, at this pH 32% of rhodopsin would be protonated in the ground state; therefore we would expect the uptake of 0.68 H^+/MII.

Implications for GPCRs. Although there is not high overall sequence homology among GPCRs, limited regions are highly conserved. One of these is the portion of the second intracellular loop at the end of helix 3, which contains the E(D)RY sequence (*76*, *77*). This maps to Glu-134 of rhodopsin, the potential protonation site required for MII formation (*35*). Opsin mutants, wherein a neutral amino acid replaces Glu-134, show enhanced G protein activation (*51*, *52*) suggesting that neutralization of this charge is necessary for the receptor's active configuration.

Neutral amino acid mutations of the Asp in the DRY sequence of other GPCRs also produce constitutive activity. Mutational analysis in conjunction with molecular modeling suggests that protonation of Asp in the DRY sequence is required for activation of α_{1B}-adrenergic (*78*, *79*), β_2-adrenergic (*80*), and gonadotropin-releasing-hormone receptors (*81*). This suggests the possibility of MI- and MII-like states in other GPCRs.

Phosphorylation of GPCRs is a paradigm for receptor deactivation. Phosphorylation lowers local membrane surface potential resulting in lower local membrane pH. This could favor protonation of Glu or Asp in the E(D)RY sequence, thereby stabilizing the MII-like conformation of other receptors.

Though not discussed by the authors, Figures 1 and 4 from Gurevich et al. (*82*) show that phosphorylated β_2-adrenergic and m2 muscarinic cholinergic receptors do not have increased affinity for agonist compared to unphosphorylated receptors. Since these receptors were reconstituted into PC vesicles, they are predicted not to undergo an appreciable change in membrane surface pH upon phosphorylation. As discussed above, rhodopsin reconstituted into PC vesicles also fails to show a phosphorylation-dependent change in MI−MII equilibrium (*17*).

Scheme 2 suggests that the p*K* of Glu-134 may shift from 5.0 to 6.3 upon receptor activation. Protonation of the corresponding site in other GPCRs appears important in converting the receptor from the inactive to active conforma-

tion. An increase in p*K* of Asp or Glu in the E(D)RY sequence upon agonist binding may serve as a general mechanism of GPCR activation.

In conclusion, we have shown that rhodopsin phosphorylation stabilizes the active conformation of rhodopsin, MII, by augmenting the negative RDM surface potential. The increase in negative membrane surface potential through receptor phosphorylation could have other important functions in visual signaling and be another paradigm for regulation of GPCR signaling.

ACKNOWLEDGMENT

We are grateful to Dr. Kim Sharp for helpful discussions and advice. We thank Professor Rosalie Crouch for kindly providing 11-*cis*-retinal.

REFERENCES

1. Matthews, R. G., Hubbard, R., Brown, P. K., and Wald, G. (1963) *J. Gen. Physiol. 47*, 215−240.
2. Emeis, D., Kuhn, H., Reichert, J., and Hofmann, K. P. (1982) *FEBS Lett. 143*, 29−34.
3. Bennett, N., Michel-Villaz, M., and Kuhn, H. (1982) *Eur. J. Biochem. 127*, 97−103.
4. Kibelbek, J., Mitchell, D. C., Beach, J. M., and Litman, B. J. (1991) *Biochemistry 30*, 6761−6768.
5. Abrahamson, E. W., and Wiesenfeld, J. R. (1972) in *Handbook of Sensory Physiology* (Dartnall, J. A., Ed.) pp 69−121, Springer-Verlag, West Berlin.
6. Parkes, J. H., and Liebman, P. A. (1984) *Biochemistry 23*, 5054−5061.
7. Liebman, P. A., and Pugh, E. N., Jr. (1979) *Vision Res. 19*, 375−380.
8. Liebman, P. A., and Pugh, E. N., Jr. (1980) *Nature 287*, 734−736.
9. Sitaramayya, A., and Liebman, P. A. (1983) *J. Biol. Chem. 258*, 1205−1209.
10. Kühn, H., and Dreyer, W. J. (1972) *FEBS Lett. 20*, 1−6.
11. Bownds, D., Dawes, J., Miller, J., and Stahlman, M. (1972) *Nature 237*, 125−127.
12. Frank, R. N., Cavanagh, H. D., and Kenyon, K. R. (1973) *J. Biol. Chem. 248*, 596−609.
13. Sitaramayya, A. (1986) *Biochemistry 25*, 5460−5468.
14. Wilden, U., Hall, S. W., and Kuhn, H. (1986) *Proc. Natl. Acad. Sci. U.S.A. 83*, 1174−1178.
15. Bennett, N., and Sitaramayya, A. (1988) *Biochemistry 27*, 1710−1715.
16. Gibson, S. K., Parkes, J. H., and Liebman, P. A. (1998) *Biochemistry 37*, 11393−11398.
17. Mitchell, D. C., Kibelbek, J., and Litman, B. J. (1992) *Biochemistry 31*, 8107−8111.
18. Tsui, F. C., Sundberg, S. A., and Hubbell, W. L. (1990) *Biophys. J. 57*, 85−97.
19. Gibson, N. J., and Brown, M. F. (1991) *Biochem. Biophys. Res. Commun. 176*, 915−921.
20. McLaughlin, S. (1977) *Curr. Top. Membr. Transp. 9*, 71−144.
21. McLaughlin, S. (1989) *Annu. Rev. Biophys. Biophys. Chem. 18*, 113−136.
22. Hubbell, W. L. (1990) *Biophys. J. 57*, 99−108.
23. Koutalos, Y., Ebrey, T. G., Gilson, H. R., and Honig, B. (1990) *Biophys. J. 58*, 493−501.
24. Cafiso, D. S. (1991) *Curr. Opin. Struct. Biol. 1*, 185−190.
25. LaTorre, R., Labarca, P., and Naranjo, D. (1992) *Methods Enzymol. 207*, 471−501.
26. Denisov, G., Wanaski, S., Luan, P., Glaser, M., and McLaughlin, S. (1998) *Biophys. J. 74*, 731−744.
27. Yee, R., and Liebman, P. A. (1978) *J. Biol. Chem. 253*, 8902−8909.
28. Knowles, A., and Dartnall, J. A. (1977) in *The Eye* (Davson H., Ed.) pp 53−101, Academic Press, New York.
29. Parkes, J. H., and Liebman, P. A. (1994) *Biophys. J. 66*, 80−88.
30. Emeis, D., and Hofmann, K. P. (1981) *FEBS Lett. 136*, 201−207.
31. Good, N. E., and Izawa S. (1972) in *Methods in Enzymology* (San Pietro, A., Ed.) Vol. 24B, pp 53−74, Academic Press, New York.
32. Liebman, P. A., Parker, K. R., and Dratz, E. A. (1987) *Annu. Rev. Physiol. 49*, 765−791.
33. Cantor, C., and Schimmel, P. (1980) in *Biophysical Chemistry, Part I. The Conformation of Biological Macromolecules*, Freeman Publications, San Francisco, CA.
34. Izatt, R. M., and Christensen, J. J. (1970) in *CRC Handbook of Biochemistry* (Sober, H. A., Ed.) pp 58−174, The Chemical Rubber Co., Cleveland, OH.
35. Arnis, S., Fahmy, K., Hofmann, K. P., and Sakmar, T. P. (1994) *J. Biol. Chem. 269*, 23879−23881.
36. Tsui, F. C., Ojcius, D. M., and Hubbell, W. L. (1986) *Biophys. J. 49*, 459−468.
37. Eisenberg, M., Gresalfi, T., Riccio, T., and McLaughlin, S. (1979) *Biochemistry 18*, 5213−5223.
38. Jager, S., Szundi, I., Lewis, J. W., Mah, T. L., and Kliger, D. S. (1998) *Biochemistry 37*, 6998−7005.
39. Delange, F., Merkx, M., Bovee-Geurts, P. H., Pistorius, A. M., and Degrip, W. J. (1997) *Eur. J. Biochem. 243*, 174−180.
40. Kuhn, H., Hall, S. W., and Wilden, U. (1984) *FEBS Lett. 176*, 473−478.
41. Cafiso, D. S., and Hubbell, W. L. (1980) *Biophys. J. 30*, 243−263.
42. Bennett, N. (1980) *Eur. J. Biochem. 111*, 99−103.
43. Apell, H. J., Bamberg, E., Alpes, H., and Lauger, P. (1977) *J. Membr. Biol. 31*, 171−188.
44. Cai, M., and Jordan, P. C. (1990) *Biophys. J. 57*, 883−891.
45. Ohguro, H., Van Hooser, J. P., Milam, A. H., and Palczewski, K. (1995) *J. Biol. Chem. 270*, 14259−14262.
46. Hurley, J. B., Spencer, M., and Niemi, G. A. (1998) *Vision Res. 38*, 1341−1352.
47. Zhang, L., Sports, C. D., Osawa, S., and Weiss, E. R. (1997) *J. Biol. Chem. 272*, 14762−14768.
48. Brannock, M. T., Weng, K., and Robinson, P. R. (1999) *Biochemistry 38*, 3770−3777.
49. MyersPayne, S. C., Mitchell, D. C., and Litman, B. J. (1996) *Biophys. J. 70*, WPO95−WPO95.
50. Radding, C. M., and Wald, G. (1956) *J. Gen. Physiol. 39*, 909−922.
51. Fahmy, K., and Sakmar, T. P. (1993) *Biochemistry 32*, 7229−7236.
52. Cohen, G. B., Yang, T., Robinson, P. R., and Oprian, D. D. (1993) *Biochemistry 32*, 6111−6115.
53. Weitz, C. J., and Nathans, J. (1993) *Biochemistry 32*, 14176−14182.
54. Buczylko, J., Saari, J. C., Crouch, R. K., and Palczewski, K. (1996) *J. Biol. Chem. 271*, 20621−20630.
55. Zhukovsky, E. A., and Oprian, D. D. (1989) *Science 246*, 928−930.
56. Sakmar, T. P., Franke, R. R., and Khorana, H. G. (1989) *Proc. Natl. Acad. Sci. U.S.A. 86*, 8309−8313.
57. Nathans, J. (1990) *Biochemistry 29*, 9746−9752.
58. Weitz, C. J., and Nathans, J. (1992) *Neuron 8*, 465−472.
59. Arnis, S., and Hofmann, K. P. (1993) *Proc. Natl. Acad. Sci. U.S.A. 90*, 7849−7853.
60. Thorgeirsson, T. E., Lewis, J. W., Wallace-Williams, S. E., and Kliger, D. S. (1993) *Biochemistry 32*, 13861−13872.
61. Kawamura, S. (1993) *Nature 362*, 855−857.
62. Chen, C. K., Inglese, J., Lefkowitz, R. J., and Hurley, J. B. (1995) *J. Biol. Chem. 270*, 18060−18066.
63. Klenchin, V. A., Calvert, P. D., and Bownds, M. D. (1995) *J. Biol. Chem. 270*, 16147−16152.
64. Koch, K. W., and Stryer, L. (1988) *Nature 334*, 64−66.
65. Kutuzov, M. A., and Bennett, N. (1996) *Eur. J. Biochem. 238*, 613−622.
66. Straume, M., Mitchell, D. C., Miller, J. L., and Litman, B. J. (1990) *Biochemistry 29*, 9135−9142.

67. Szundi, I., Mah, T. L., Lewis, J. W., Jager, S., Ernst, O. P., Hofmann, K. P., and Kliger, D. S. (1998) *Biochemistry 37*, 14237−14244.
68. Dickopf, S., Mielke, T., and Heyn, M. P. (1998) *Biochemistry 37*, 16888−16897.
69. King, P. J., and Gutfreund, H. (1984) *Vision Res. 24*, 1471−1475.
70. Baumann, C., and Zeppenfeld, W. (1981) *J. Gen. Physiol 317*, 347−364.
71. Bennett, N. (1978) *Biochem. Biophys. Res. Commun. 83*, 457−465.
72. McConnell, D. G., Rafferty, C. N., and Dilley, R. A. (1968) *J. Biol. Chem. 243*, 5820−5826.
73. Wong, J. K., and Ostroy, S. E. (1973) *Arch. Biochem. Biophys. 154*, 1−7.
74. Cooper, A., and Converse, C. A. (1976) *Biochemistry 15*, 2970−2978.
75. Cooper, A., and Johnson, C. M. (1994) in *Microscopy, Optical Spectroscopy, and Macroscopic Techniques* (Jones, C., Mulloy, B., and Thomas, A. H., Eds.) pp 125−136, Humana Press, Totowa, NJ.
76. Dohlman, H. G., Thorner, J., Caron, M. G., and Lefkowitz, R. J. (1991) *Annu. Rev. Biochem. 60*, 653−688.
77. Probst, W. C., Snyder, L. A., Schuster, D. I., Brosius, J., and Sealfon, and S. C. (1992) *DNA Cell Biol. 11*, 1−20.
78. Scheer, A., Fanelli, F., Costa, T., De Benedetti, P. G., and Cotecchia, S. (1996) *EMBO J. 15*, 3566−3578.
79. Scheer, A., Fanelli, F., Costa, T., De Benedetti, P. G., and Cotecchia, S. (1997) *Proc. Natl. Acad. Sci. U.S.A. 94*, 808−813.
80. Gether, U., and Kobilka, B. K. (1998) *J. Biol. Chem. 273*, 17979−17982.
81. Ballesteros, J., Kitanovic, S., Guarnieri, F., Davies, P., Fromme, B. J., Konvicka, Chi, L., Millar, R. P., Davidson, J. S., Weinstein, H., and Sealfon, S. C. (1998) *J. Biol. Chem. 273*, 10445−10453.
82. Gurevich, V. V., Pals-Rylaarsdam, R., Benovic, J. L., Hosey, M. M., and Onorato, J. J. (1997) *J. Biol. Chem. 272*, 28849−28852.

BI990411W